Magnetic phase diagram of $Nd_{0.5}Sr_{0.5}MnO_3$ probed by ^{17}O NMR

A. Trokiner,[1] S. Verkhovskii,[1,2] A. Yakubovskii,[1,3] K. Kumagai,[4] P. Monod,[1] K. Mikhalev,[2] A. Buzlukov,[2] Y. Furukawa,[4] N. Hur,[5] and S.-W. Cheong[5]

[1]*Laboratoire de Physique du Solide, ESPCI, UPR CNRS A05, Paris 75231, France*

[2]*Institute of Metal Physics, Ural Branch of Russian Academy of Sciences, Ekaterinburg 620041, Russia*

[3]*Russian Research Centre "Kurchatov Institute," Moscow 123182, Russia*

[4]*Division of Physics, Graduate School of Sciences, Hokkaido University, Sapporo 060-0810, Japan*

[5]*Rutgers Center for Emergent Materials and Department of Physics and Astronomy, Rutgers University, Piscataway, New Jersey 08854, USA*

(Received 1 December 2007; published 18 April 2008)

We have used ^{17}O NMR to probe the magnetic homogeneity in both the paramagnetic and the ferromagnetic states of a high-quality $Nd_{0.5}Sr_{0.5}MnO_3$ single crystal. The measured broadening of the ^{17}O line reveals that significant two-dimensional static correlations of neighboring Mn spins in the *ab* planes exist in the paramagnetic phase far above the transition. Our results also indicate that the ferromagnetic metallic state at low temperatures, resulting from the melting of the charge ordered (charge-exchange type) insulating state in 94 kOe, is rather inhomogeneous: regions with almost perfect long-ranged ferromagnetic order coexist with regions with poor ferromagnetic (FM) order. The latter regions represent about 25% of the sample and are due to inherent structural strains inside the FM domain.

DOI: 10.1103/PhysRevB.77.134436 PACS number(s): 75.25.+z, 71.30.+h, 75.40.Cx, 76.60.−k

I. INTRODUCTION

The doped manganite perovskites show a complex phase diagram with many coexisting phases, in which electronic and structural properties relate to the physics of strongly correlated materials.[1–3] The fine balance between the kinetic energy and Coulomb interaction of electrons in the partially filled, high-spin $3d$(Mn)-$2sp$(O) band results at low temperature in several possible ground states, mainly the ferromagnetic three-dimensional (3D) metallic (FMM), the antiferromagnetic two-dimensional (2D) metallic (AFM *A*-type), and the antiferromagnetic charge ordered (CO) insulating states. The ground state of half-doped compounds, where the rational fraction of doped electrons per Mn ion provides macroscopic stability of the antiferromagnetic (AF) insulating charge-exchange (CE) phase, demonstrates the simultaneous charge ordering (Mn^{3+}/Mn^{4+}), orbital ordering (OO), and magnetic ordering.[4,5] The CE-type CO/OO order implies a ferromagnetic (FM) zigzag arrangement of the ordered $e_g(3x^2-r^2)$ and $e_g(3y^2-r^2)$ orbitals of Mn^{3+} ions in the *ab* plane, as shown in Fig. 1. The neighboring zigzags are AF coupled; the ordering in the *c* direction is also AF.

In nearly half-doped $Nd_{1-x}Sr_xMnO_3$, the FMM and AFM *A*-type phases lay very close in energy [the energy difference of ~0.01 eV/Mn (Ref. 6)] to the insulating CE phase. At low temperature and for $x \leqslant 0.48$, $Nd_{1-x}Sr_xMnO_3$ is in the FMM phase, and for $x \geqslant 0.51$, it is in the AFM *A*-type phase so that the CE phase exists in a very narrow concentration range, $0.48 < x < 0.51$.[7]

In the absence of magnetic field, the nominally half-doped ($x=0.50$) oxide undergoes two phase transitions, first from a paramagnetic insulating (PI) to the FMM phase (both of the orthorhombic *Imma* symmetry) at $T_C \sim 250$ K, then to the AF insulating CE phase (monoclinic $P2_1/m$ structure) at $T_N \sim 160$ K. The coexistence of the competing FMM, AFM (*A* type) and CE phases was deduced from low-field magnetization and magnetostriction studies[8] and confirmed directly by x-ray and neutron diffraction techniques.[9,10]

In addition, nanoscale structural inhomogeneities were evidenced by x-ray scattering in the FMM and PI phases of a $Nd_{0.5}Sr_{0.5}MnO_3$ single crystal. In the FMM state,[11] short-range orbital correlations were predominantly detected in the *ab* plane. It was suggested that the PI phase far above T_C as well as the FMM phase exhibit local regions with layered orbital order.[12,13]

The magnetic character of these structurally inhomogeneous regions is important considering that transport properties are mainly determined by the spin dependent scattering of charge carriers in the conducting band. Not many experimental studies of the magnetic character of these inhomogeneities are reported. The spin dynamic of magnetic ions was

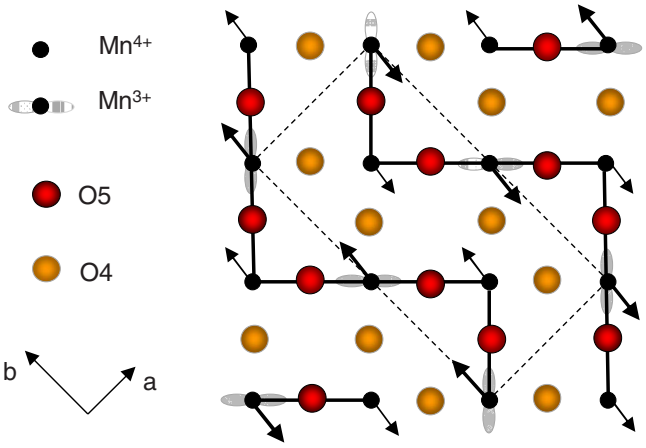

FIG. 1. (Color online) CE-type magnetic structure in the *ab* plane is shown for CO state of $Nd_{0.5}Sr_{0.5}MnO_3$. The ferromagnetic zigzags are indicated by the solid lines, and the dotted rectangle indicates the low temperature unit cell. The arrows show the Mn spins orientations.

investigated in $Nd_{0.5}Sr_{0.5}MnO_3$ by muon spin relaxation spectroscopy[14] and the inelastic neutron scattering technique.[15] It was shown that a prominent 2D FM component coexists with the conventional isotropic quasielastic ($q \sim 0$) background in the spectrum of spin fluctuations in the PI phase.

In this paper, static magnetic inhomogeneities probed by ^{17}O NMR are considered. These inhomogeneities are evidenced in both the PI and the FMM states of a high-quality $Nd_{0.5}Sr_{0.5}MnO_3$ sample under an applied magnetic field.

II. EXPERIMENTAL DETAILS

The twinned single crystal that is used for this study (plate of $6 \times 4 \times 2$ mm^3) belongs to the same batch as the $Nd_{0.5}Sr_{0.5}MnO_3$ single crystal used in the x-ray structural studies.[12] Its magnetic characterization was performed in a magnetic field of 100 Oe with a superconducting quantum interference device (SQUID) magnetometer (MPMS-5T, "Quantum Design"). In Fig. 2(a), the curves clearly show two magnetic transitions of the sample. On cooling, the Curie point is at $T_C = 251(2)$ K and the FMM-AF CE transition is at $T_N = 155(2)$ K. The single crystal was then crushed into a powder with grain size of about 20 μm in order to prepare a homogeneously ^{17}O enriched NMR sample. The powder was enriched up to $\sim 15\%$ by heating at 930 °C for 140 h in a flow of oxygen gas ($P_{O_2} \approx 1.5$ bar). At this annealing temperature, it is well known[16–18] that the cationic content of refractory manganites such as $Nd_{0.5}Sr_{0.5}MnO_3$ is not changed. The level of 17-oxygen enrichment was controlled in test experiments by weighting the sample. For similarly sized powder, we definitely got the mass saturation after several hours of heat treatment with (T, P_{O_2}) parameters used in this work.

The bulk magnetization $M(T; H = 100$ Oe) data of the ^{17}O enriched powder presented in Fig. 2(b) show the two magnetic transitions at $T_C = 249.2(20)$ K and $T_N = 160(2)$ K. The sharpness of the transitions is the same as in the starting crystal [Fig. 2(a)]. A small increase of T_N in the ^{17}O enriched sample compared to the starting crystal is measured. In the former, the long heat treatment in oxygen atmosphere may induce a slightly different oxygen stoichiometry compared to the starting crystal. The small shift of T_C should be addressed to the difference in the oxygen stoichiometry rather than to a ^{17}O-^{16}O isotope effects.[35]

The NMR measurements at $H = 0$ and 94 kOe were performed with pulse phase-coherent spectrometers; the 117.4 kOe data were acquired on the Bruker ASX500 spectrometer. The ^{17}O NMR spectra were obtained by measuring at each frequency (ν) the spin-echo intensity obtained with the pulse sequence $(\pi/2)$-t_{del}-(π)-echo. The width of the $\pi/2$ pulse did not exceed 1.5 μs. The intensity of the ^{17}O echo signals were corrected to $t_{del} = 0$ after measuring the echo-decay rate at different frequencies of the spectrum. The quality factor of the NMR coil, the 50 Ω impedance of the resonant circuit, and the gain of the rf pulse were kept constant through the wide spectrum. The ^{17}O spectral intensity shown in the figures is the measured echo signal intensity multiplied by ν^{-2}. Thus the fraction of oxygen contributing to the signal at a given frequency is directly obtained. The ^{17}O NMR signal in H_2O was used as a frequency reference to determine the shift of the NMR line.

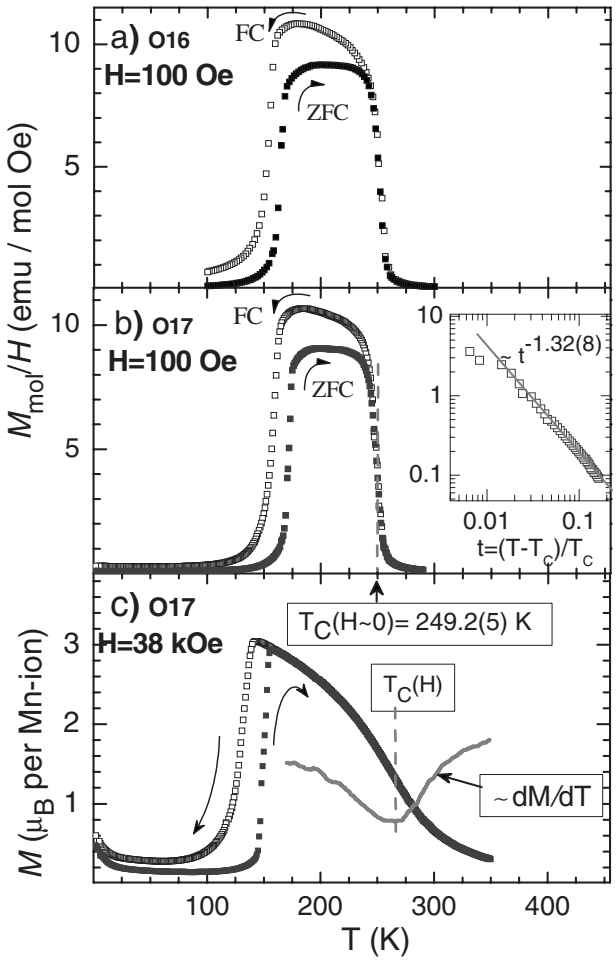

FIG. 2. [(a) and (b)] Magnetization $M(T)$ of $Nd_{0.5}Sr_{0.5}MnO_3$ measured by SQUID in the ZFC-FC thermal cycle (shown by arrows) in the starting crystal at magnetic field (a) $H = 100$ Oe, and in the ^{17}O enriched crushed crystal at magnetic field (b) $H = 100$ Oe and (c) 38 kOe. The details of critical behavior M vs $t = (T - T_C)/T_C$ in the paramagnetic phase are shown in the inset; the solid line is a linear fit of $M(t; H = 100$ Oe) data presented in the double logarithmic scale. The maximum of the derivative dM/dT indicates $T_C(H)$, the crossover temperature for PI-FMM transition at $H = 38$ kOe.

III. RESULTS AND DISCUSSION

A. The paramagnetic and ferromagnetic states above T_N

The temperature dependence of $M(T)$ in zero field cooled (ZFC) and field cooled (FC) runs in the magnetic fields $H = 0.1$ and 38 kOe, which is shown in Figs. 2(b) and 2(c). The reversible behavior observed on the ZFC-FC thermal cycle near the transition from the PI to FMM state confirms a characteristic feature of second order phase transitions. The magnetization $M(t; H = 100$ Oe) with $t = (T - T_C)/T_C$ and $t < 0.1$ presented in the inset of Fig. 2(b) follows a power law dependence $M(t) \sim t^{-\gamma}$. The critical exponent $\gamma = 1.32(8)$ is

consistent with the 3D Heisenberg model for magnetic systems with isotropic exchange interaction ($\gamma_{theor}=1.33$). At high magnetic field, although the phase transition is no longer thermodynamically defined, the characteristic temperature $T_C(H)$ of the crossover from the PI to FMM phase is conventionally defined as the inflection point, $\max|M'(T)|$, of the $M(T)$ curve. At 38 kOe, the transition is shifted above $T_C(H\sim 0)$ by $\Delta T_C\sim(15-20)$ K [Fig. 2(c)].

Let us turn to ^{17}O NMR results in the PI phase. The oxygen ion is placed between two Mn ions in the perovskite structure and each ^{17}O nucleus probes the spin and orbital configurations of the corresponding Mn pair through the transferred spin density.[19,20] The resulting ^{17}O spectrum is a superposition of several lines. The intensity, position, and width of each line depend on the specific spatial distribution of the static spin correlations $\langle \boldsymbol{S}(\mathrm{Mn}_i)\boldsymbol{S}(\mathrm{Mn}_j)\rangle$ in the crystal. In doped manganites, the local magnetic field at O sites $\boldsymbol{h}_{\mathrm{loc}}$ originates mainly from the Fermi-contact interaction with the transferred s-spin density of electrons participating in the Mn-O-Mn bonding, and $\boldsymbol{h}_{\mathrm{loc}}$ may be written as

$$\boldsymbol{h}_{\mathrm{loc}} = H_{FC}(2s)\sum_{i=1,2} f_{s,i}\langle \boldsymbol{S}(\mathrm{Mn}_i)\rangle, \tag{1}$$

where $\mu_{eff}(\mathrm{Mn})=g_e\mu_B\langle S(\mathrm{Mn})\rangle$ is the effective magnetic moment of the Mn ion. The angular brackets denote an equilibrium ensemble average. $H_{FC}(2s)\equiv(8\pi/3)g_e\mu_B|\phi_{2s}(0)|^2 = 1.1$ MOe (Ref. 21) is the hyperfine magnetic field due to the Fermi-contact interaction with one unpaired electron that is located on the $2s$ orbital with wave function $\phi_{2s}(r)$. The corresponding isotropic spin density transferred to oxygen from the neighboring Mn ion is usually defined in terms of the factor $f_s=h_{\mathrm{loc}}/H_{FC}(2s)$ for $\mu_{eff}=1\mu_B$.[22] The positive or negative sign of f_s is determined by the peculiar covalent mixing of the $2s$(O) orbital with the partially filled and/or empty e_g(Mn) orbital.[19,23]

The ^{17}O spectra, which are measured at $H=94$ kOe in the PI and FMM phases of $Nd_{0.5}Sr_{0.5}MnO_3$, are shown in Fig. 3. Each spectrum consists of a single line, indicating that all Mn ions are equivalent. Let us first consider the behavior of the average local field h_{loc} measured at the maximum of the symmetric line. In the PI phase, the static part of the local field reduces to its projection $h_{\mathrm{loc},z}$ along $H\|z$; Eq. (1) takes a scalar form

$$h_{\mathrm{loc},z}(T) = 2f_sH_{FC}(2s)\langle S_z(\mathrm{Mn})\rangle. \tag{2a}$$

As shown in the inset, with decreasing temperature, the average local field increases following the Curie-Weiss law $h_{\mathrm{loc},z}^{-1}\sim(T-\theta_{\mathrm{NMR}})$ with $\theta_{\mathrm{NMR}}=270(10)$ K. This value is close to $T_C(H)$, which is deduced from macroscopic magnetization data at $H=38$ kOe [Fig. 2(c)]. The mean-field-like behavior of $h_{\mathrm{loc}}(T)$ with $\theta_{\mathrm{NMR}}\simeq T_C(H)$ indicates that $\langle S_z(\mathrm{Mn})\rangle$ is proportional to $M(T)=\chi_s(T;q=0)H$ and thus

$$h_{\mathrm{loc},z}(T) = 2f_sH_{FC}(2s)\chi_s(T;q=0)H/\mu_B, \tag{2b}$$

where $\chi_s(T;q=0)$ is the uniform part of the spin susceptibility $\chi_s(T;q)$. This was also reported in Ref. 15 for the PI state at $H=0$ of a $Nd_{0.5}Sr_{0.5}MnO_3$ single crystal where the Mn spin fluctuation spectrum is dominated by the diffusive component $\chi_s(q\sim 0)$. Considering its averaged properties, $M(T)$

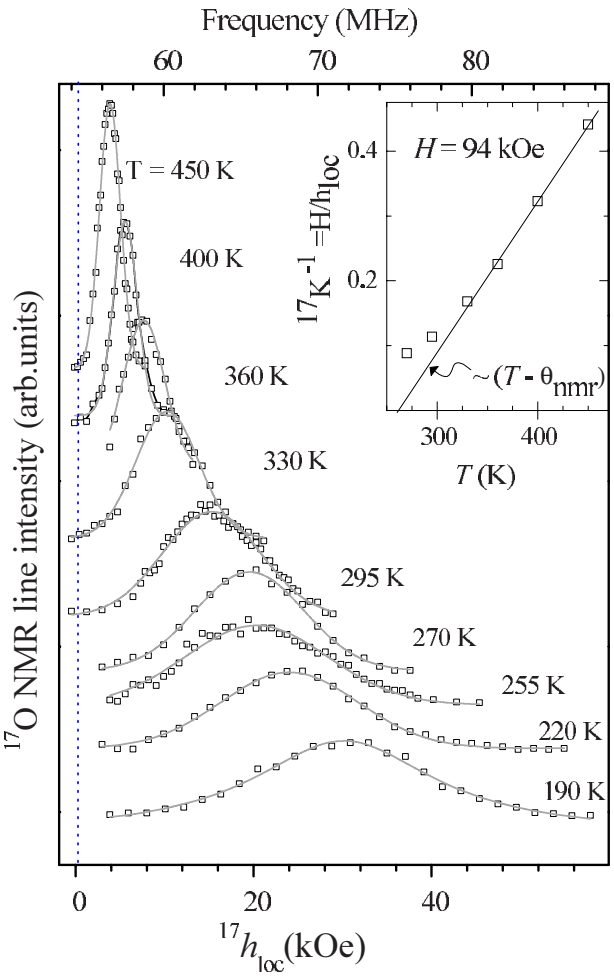

FIG. 3. (Color online) ^{17}O NMR spectra measured at $H=94$ kOe in the PI and FMM phases of $Nd_{0.5}Sr_{0.5}MnO_3$. The corresponding gray curves are the result of a Gaussian fit of the data (□). The vertical doted line shows the position of ^{17}O NMR line in the standard reference H_2O ($h_{\mathrm{loc}}=0$). The temperature dependence of the inverse ^{17}O NMR line shift, $^{17}K=h_{\mathrm{loc}}/H$, and the corresponding linear fit (solid line) are shown in the inset.

and $h_{\mathrm{loc},z}$, our sample behaves as a homogeneous bulk paramagnet undergoing a FM transition.

The width at half height of the ^{17}O NMR line (δh) increases likewise with decreasing temperature. The ratio $(\delta h)/h_{\mathrm{loc}}$ vs T is shown in Fig. 4(a) for the PI state of $Bi_{0.5}Ca_{0.5}MnO_3$ (Ref. 24) and $Nd_{0.5}Sr_{0.5}MnO_3$. The former undergoes a first order phase transition from the PI to a CO state at 330 K, and the latter a second order phase transition to the FMM state. The temperature dependence of the ratio $(\delta h)/h_{\mathrm{loc}}$ is remarkably different in the PI phase. $Bi_{0.5}Ca_{0.5}MnO_3$ shows a T-independent $(\delta h)/h_{\mathrm{loc}}$, whereas a 50% growth is observed for $Nd_{0.5}Sr_{0.5}MnO_3$ as the temperature decreases.

Two main origins of the T-dependent magnetic broadening should be considered for the ^{17}O NMR line in the paramagnetic state of a powder sample. One origin is due to classic demagnetizing fields[25] and the other to static Mn-Mn spin correlations,[26] yielding an upturn at $q\neq 0$ of the magnetic response function $\chi_s(q)=\chi_s(q$

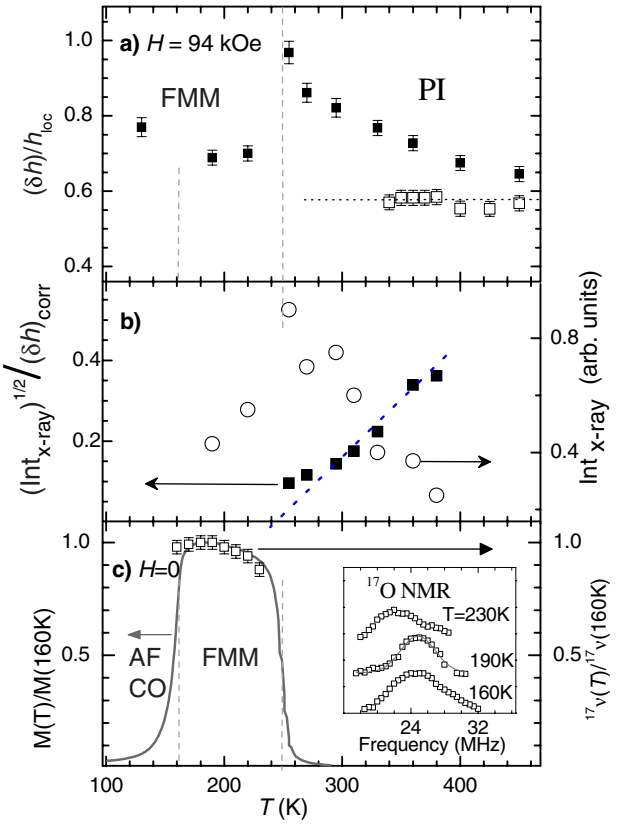

FIG. 4. (Color online) (a) Thermal dependence of the ^{17}O NMR line width (δh) divided by the averaged $h_{\rm loc}$ measured at $H=94$ kOe in $Nd_{0.5}Sr_{0.5}MnO_3$ (■) and $Bi_{0.5}Ca_{0.5}MnO_3$ (□) manganites. (b) The ratio $\{\mathrm{Int}_{x-ray}/(\delta h)^2_{\rm corr}\}^{1/2}$ displays the same thermal variation as the inverse spin susceptibility of the correlated neighboring Mn-Mn in the PI phase of $Nd_{0.5}Sr_{0.5}MnO_3$. The data Int_{x-ray} are taken from Fig. 3 of Ref. 13. (c) The thermal variation of the relative resonance frequency $^{17}\nu(T)/^{17}\nu(160\ \mathrm{K})$ of ^{17}O NMR line (see inset) measured on cooling in the FMM phase at $H=0$ is compared to the thermal behavior of the macroscopic magnetization $M(T;H=100$ Oe).

$=0)\Sigma_{i,j}[\langle S_z(\mathrm{Mn}_i)S_z(\mathrm{Mn}_j)\rangle e^{i\mathbf{q}\mathbf{r}_{ij}}-\langle S_z^2(\mathrm{Mn}_i)\rangle]$. Within the Gaussian approximation, the ^{17}O linewidth can be written in the form

$$(\delta h)=\{(\delta h)^2_{\rm demagn}+(\delta h)^2_{\rm corr}\}^{0.5}. \tag{3}$$

The first contribution $(\delta h)_{\rm demagn}=\langle N\rangle\chi_{\rm vol}H$ is proportional to the magnetic field and the measured volume susceptibility $\chi_{\rm vol}\sim M(T)/H$. This classic magnetic broadening is an intrinsic property of the spatially uniform paramagnet whose magnetic fluctuations are controlled by $\chi_s(q=0)\sim(T-\theta)^{-1}$. The corresponding ratio $(\delta h)_{\rm demagn}/h_{\rm loc}$ is temperature independent. $\langle N\rangle$ is the demagnetizing factor averaged over all crystallites.[25] An accurate estimate of $\langle N\rangle$ is difficult. We rather get a range $(\delta h)_{\rm demagn}=(0.5-0.7)h_{\rm loc}$ for our $Nd_{0.5}Sr_{0.5}MnO_3$ sample. For $Bi_{0.5}Ca_{0.5}MnO_3$, the experimental value $(\delta h)/h_{\rm loc}=0.58(4)$ lies inside this range. As $(\delta h)/h_{\rm loc}$ is T independent, it is explicitly due to demagnetizing effects. We will assume that for our $Nd_{0.5}Sr_{0.5}MnO_3$ powder sample $(\delta h)_{\rm demagn}=0.58h_{\rm loc}$.

As shown in Figs. 4(a) and 4(b), the increase of the magnetic broadening occurs in the same range of temperature where a considerable growth of the x-ray intensity Int_{x-ray} of the Bragg peak due to short-range structural correlations is observed in a $Nd_{0.5}Sr_{0.5}MnO_3$ single crystal.[12,13] The symmetry of these nanoregions is different from the average *Imma* lattice symmetry. The quantity Int_{x-ray} is proportional to the concentration of these correlated layered regions. We suggest that there is a one to one correspondence between the short-range structural order probed by x-ray diffusive scattering (Fig. 2 of Ref. 13) and the magnetic inhomogeneities revealed by ^{17}O NMR measurements.

In order to elucidate the type of magnetic order for Mn spins in these correlated nanoregions, let us consider the second term in Eq. (3). It represents the summation on oxygen sites with different sorts of static pair correlation i of the two nearest Mn-spin neighbors S_1 and S_2,

$$(\delta h)^2_{\rm corr}=\sum_i c_i(\delta h)^2_{i,\rm corr}, \tag{4a}$$

$$(\delta h)^2_{i,\rm corr}=f_{s1}f_{s2}H_{FC}(2s)[\langle S_{z1}S_{z2}\rangle-\langle S_{z1}\rangle\langle S_{z2}\rangle]. \tag{4b}$$

The extra broadening of the ^{17}O NMR line due to Mn-Mn correlations is proportional to $\sqrt{c_i}$, where c_i is the concentration of specifically correlated Mn-spin pairs. At high temperature, the correlations are thermally destroyed and $\langle S_{z1}S_{z2}\rangle=\langle S_{z1}\rangle\langle S_{z2}\rangle=1/3S(S+1)\delta_{12}$ so that $(\delta h)^2_{\rm corr}$ vanishes.

We discuss the possible Mn spin correlations which are responsible of this extra broadening. In all 3D CO-OO phases of half-doped manganites, the neighboring Mn ions with the same valence have AF correlated spins. Each Mn of the pair creates at the oxygen in the center a local field with the same magnitude but with opposite sign.[19,20] As a result, an additional NMR line peaked at $h_{\rm loc}\sim 0$ should be formed by this oxygen. The absence of NMR signal at $h_{\rm loc}\sim 0$ (Fig. 3) excludes any static 3D orbital ordered configurations in the PI state. Nevertheless, the following CO and/or OO configurations of neighboring Mn with a reduced dimensionality can be counted. Indeed, the 2D orbital order existing in the *ab* plane of the CE structure (Fig. 1) and the one occurring in the ferromagnetically ordered layers of the AFM *A*-type phase provide a positive contribution to $(\delta h)^2_{\rm corr}$. In the PI phase with average crystal symmetry (*Imma*), one should expect that in these regions where static 2D magnetic order occurs the new magnetic structure is accompanied with local structural distortions related to the OO order. It is consistent with x-ray structural[12,13] and neutron scattering[15] results. Assuming that the thermal dependence of c_i scales that of Int_{x-ray},[13] the ratio $m_{\rm corr}=\{(\delta h_{\rm corr})^2/\mathrm{Int}_{x-ray}\}^{1/2}$ should track the thermal variation of $\langle S_{z1}S_{z2}\rangle$, yielding unique information on the short wave component $q=\pi/r_{12}$ of the static magnetic susceptibility $\chi_s(q)$, where r_{12} is the Mn-Mn distance. With decreasing temperature $m^{-1}_{\rm corr}$ gradually decreases [Fig. 4(b)]. The approximation $\chi_s^{-1}(q=\pi/r_{12})\sim(T-\theta_{\rm corr})$ leads to a positive value $\theta_{\rm corr}$. It indicates that the FM exchange interaction between neighboring Mn dominates in these regions.

Let us consider the magnetic homogeneity of our $Nd_{0.5}Sr_{0.5}MnO_3$ below T_C where the long-range ferromagnetic order is formed. The magnetization $M(H)$ isotherms

between 170 and 200 K show well saturated behavior ($dM/dT < 2\times10^{-4}\mu_B$/kOe) in magnetic field above 20 kOe, indicating that the magnetic anisotropy field is small, $H_M < 2$ kOe. This is evidence for a single domain formation at higher magnetic field.

^{17}O NMR spectra measured at 94 kOe are shown in Fig. 3. The spectrum consists of a single symmetric line confirming the magnetic equivalence of oxygen sites as expected in the single domain FMM phase. Indeed, as seen in Fig. 7, on crossing T_C the averaged local field of the line h_{loc} starts to track the thermal behavior of $M(T;38$ kOe). The corresponding ratio $(\delta h)/h_{loc}$ is substantially reduced and independent of temperature (Fig. 4). Nevertheless, a difference exists between the measured ratio $(\delta h)/h_{loc}=0.68(4)$ and $\{(\delta h)/h_{loc}\}_{demagn}=0.58$, the value expected if the FM order was perfect in this magnetically soft material. The corresponding additional broadening $(\delta h)_{FM}(H=94$ kOe) $=\{(\delta h)^2-(\delta h)_{demagn}{}^2]\}^{0.5}=0.32(2)h_{loc}$ is due to a residual intrinsic magnetic hardness. The average misalignment of the Mn magnetic moments may be represented by the angle 2α of a cone which is estimated to $2\alpha\approx\arcsin(\delta h)/h_{loc}\sim18°$ around 200 K.

At $H=0$, the intrinsic inhomogeneity inside each magnetic domain is mainly responsible for the linewidth. Some of the spectra measured at $H=0$ are shown in the inset in Fig. 4(c). Each spectrum is a single line peaked at $^{17}\nu=^{17}\gamma|h_{loc}|$, where $|h_{loc}|$ is the magnitude of the vector sum of the local fields in Eq. (1) and $^{17}\gamma$ is the gyromagnetic ratio. As seen in Fig. 4(c), the variation of $^{17}\nu(T)$ scales well $M(T)$ evidencing that the FM order remains rather uniform by switching off the magnetic field. The width of the line $(\delta h)_{FM}$ is roughly independent of T and the corresponding ratio $^{17}\delta\nu/^{17}\nu=(\delta h)_{FM}/|h_{loc}|$ is 0.30(5). The consistency of this value with $(\delta h)_{FM}(H=94$ kOe) shows that the intrinsic inhomogeneity is not changed at 94 kOe. We believe that the H-independent disordering factor preventing the perfect FM alignment among Mn spins originates in structural imperfections existing in doped manganites such as $Nd_{0.5}Sr_{0.5}MnO_3$.[3] It is worthwhile to underline that above T_N, there is no indication of another phase besides the FMM phase.

B. Ferromagnetic order at low temperature

At low magnetic field, the sharp drop of $M(T)$ below 150 K evidences the onset of long-range AF order as the CE magnetic structure occurs at low magnetic field [Figs. 2(b) and 2(c)]. The irreversibility observed in the ZFC-FC loop indicates that only a small volume fraction of the sample, $c_{V,FM}<0.05$, remains FMM down to 2 K. This phase coexistence at low T is clearly seen by ^{55}Mn NMR. We have measured the zero field NMR spectrum of ^{55}Mn ions by the spin-echo technique at 4.2 K in the same ^{17}O enriched sample. As seen in Fig. 5(a), there are two lines. The frequency position of the more intense line near 302 MHz is typical of Mn^{+4} ions in the CE phase.[27] The ^{55}Mn NMR signal of Mn^{+3} ions is not observed in the CO state of doped manganites due to the extremely fast nuclear spin-spin relaxation rate. The other line of weaker intensity is peaked at $\nu\sim375$ MHz. This line displays a very large radio-frequency

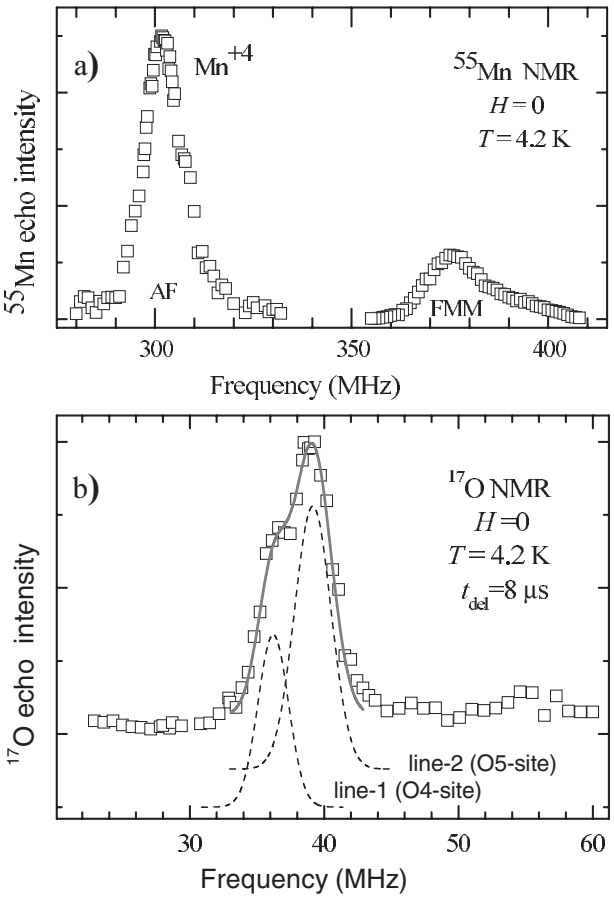

FIG. 5. NMR spectra of ^{55}Mn (a) and ^{17}O (b) measured at $H=0$ and $T=4.2$ K in the CE state of $Nd_{0.5}Sr_{0.5}MnO_3$. The contributions to ^{17}O spectral intensity of oxygen from different the two sites in the *ab* plane (see Fig. 1) are shown by two Gaussians (dotted lines).

field enhancement factor, $\eta\geqslant100$, which is typical of FM ordered regions.[22,28]

In the CO/OO phase, the splitting of the ^{17}O spectrum into several lines is expected due to the different local magnetic environments of the various O sites in the CE structure.[20,24] The ^{17}O NMR spectrum ($T=4.2$ K), as shown in Fig. 5(b), was also measured at $H=0$. By applying the spin-echo technique with variable time spacing (t_{del}) between rf pulses, the spectrum was easily decomposed into two lines with different ^{17}O spin-echo decay time T_2. The final result for the spectrum measured at $t_{del}=8$ μs is shown in Fig. 5(b), where the gray curve is a superposition of two Gaussians. The intensity of line-1 [$^{17}\nu=36$ MHz, $T_2=12(2)$ μs] and the one of line-2 [$^{17}\nu=39$ MHz, $T_2=23(2)$ μs] are in the ratio Int(line-1):Int(line-2)=1.0:0.95. This ratio is very close to the structural ratio of 1:1 for oxygen sites O4 and O5 in the *ab* plane (Fig. 1). This line assignment is the same as in other half-doped manganites.[20] The fact that no other ^{17}O line of reasonable intensity was detected is consistent with the estimate $c_{V,FM}\leqslant0.05$ of the FM phase at low temperature, showing that in zero field, the $Nd_{0.5}Sr_{0.5}MnO_3$ sample is mainly in the CE phase.[36]

Under magnetic field, $Nd_{0.5}Sr_{0.5}MnO_3$ undergoes a first order transition from the insulating CE state to the metallic

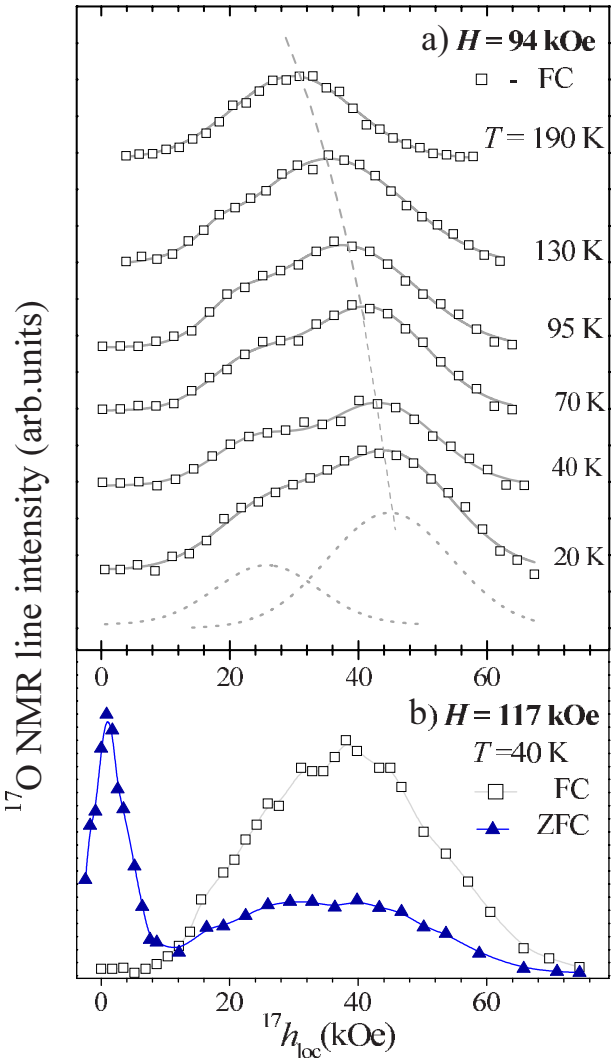

FIG. 6. (Color online) ^{17}O NMR spectra of $Nd_{0.5}Sr_{0.5}MnO_3$ measured at (a) $H=94$ kOe in the FMM phase. The solid gray curves result from the simulation of the spectra (□) by two Gaussians. The corresponding lines are shown for $T=20$ K. (b) $H=117.4$ kOe and $T=40$ K by field cooling (□) and zero field cooling (▲).

FM state so that at 94 kOe, it is expected to remain in the FMM state down to about 40 K, as it was shown from resistivity data.[29]

At 94 kOe and below 130 K, the shape of the ^{17}O NMR spectra [Fig. 6(a)] clearly becomes asymmetric compared to the Gaussian shape observed at higher temperature. The asymmetric spectra can be represented by the sum of two Gaussians centered at different h_{loc}. With decreasing temperature, the relative contribution of the line with the largest h_{loc} gradually diminishes to about 0.75 of the total intensity at $T=20$ K.

Let us analyze this more intense line. The thermal dependence of its local field $h_{loc}(T,94\ \text{kOe})$ is reported in Fig. 7 together with $M(T,38\ \text{kOe})$. At 38 kOe, the sample undergoes a phase transition from the FMM to AF CE state near 108 K, whereas at 94 kOe, it remains FMM down to 20 K. The temperature dependence of $h_{loc}(T,94\ \text{kOe})$ is satisfactory fitted up to 200 K $\approx 0.75\ T_C(H)$ with the expression usually used to analyze magnetization data of soft ferromagnets in the presence of an external magnetic field H,[30–33]

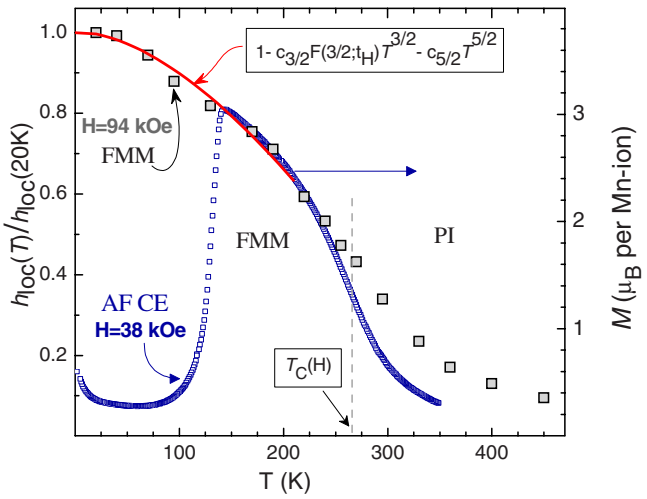

FIG. 7. (Color online) Temperature dependences of the local magnetic field at oxygen sites $h_{loc}(T)$ relative to $h_{loc}(20\ \text{K})=42$ kOe probed by ^{17}O NMR at $H=94$ kOe and of the bulk magnetization $M(T)$ measured by SQUID at $H=38$ kOe in $Nd_{0.5}Sr_{0.5}MnO_3$. Both sets of data are scaled in the FMM state. The solid curve is a fit of the NMR data with an expression in Eq. (5). The vertical gray dashed line indicates the PI-FM crossover temperature at $H=38$ kOe.

$$h_{loc}(T,H)/h_{loc}(0,H) = 1 - C_{3/2}F(3/2,k_BT/g\mu_BH)T^{3/2} - C_{5/2}T^{5/2}, \quad (5)$$

with $C_{3/2}=1.60(20)\times10^{-4}\ \text{K}^{-3/2}$ and $C_{5/2}=1.50(40)\times10^{-8}\ \text{K}^{-5/2}$. As a field of 94 kOe largely exceeds the anisotropy field $H_A\sim(10-20)$ kOe, the ferromagnetic order is almost saturated and the thermal variation of the magnetization is controlled by the modified Bloch $T^{3/2}$ term below 100 K. The factor $F(3/2,k_BT/g\mu_BH)$ is the Bose–Einstein integral function. It takes into account the gap $\Delta=g\mu_BH$, which opens in the magnon spectrum under an applied magnetic field. Assuming a cubic symmetry for the magnon dispersion curves, the estimate of the corresponding spin-wave stiffness $D(0,H=0)=140(20)$ meV Å^2 is consistent with neutron-diffraction data reported for the 3D FMM state of other doped manganites.[1,34]

In Fig. 7, the magnetization (at 38 kOe) and the local field (at 94 kOe) data are normalized in the temperature range of 160–200 K. For these temperatures and at both fields, $Nd_{0.5}Sr_{0.5}MnO_3$ is in the FMM state. The local field h_{loc} corresponds to the oxygen contributing to the more intense line [Fig. 6(a)]. The scaling shows that the FM order for these oxygens is almost saturated at 20 K with $M_{sat}=3.70(10)\mu_B/\text{Mn}$. In addition, at $T=20$ K, the ratio $(\delta h)/h_{loc}(20\ \text{K})=0.56(8)$ of this line coincides with the ratio due to demagnetization effects only. These observations mean that the corresponding oxygens are between perfectly aligned Mn magnetic moments.

The less intense line appears in the temperature region where in zero field, only the CE insulating state exists. Its local field is substantially smaller at the corresponding oxygen sites. In order to understand the origin of this line, let us consider the following scenario, which was discussed based on magnetostriction and neutron data in $Nd_{0.5}Sr_{0.5}MnO_3$. At low temperature and $H=0$, the ground state would be a phase segregated state with three magnetic structures, FMM, *A*-type AF, and CO AF CE type, the effect of high magnetic field being to transform the system into the FMM homogeneous state.[8,10] The less intense line is not consistent with the presence of regions with a 3D AF structure (*A* type or CE). The absence of any reasonable intensity of ^{17}O NMR signal around $h_{loc} \sim 0$ directly indicates that AF static correlations between Mn spins in adjacent *ab* planes do not exist. This is illustrated in Fig. 6(b), which displays the ZFC and FC spectra that are obtained at $H=117.4$ kOe and 40 K. In the ZFC procedure, the sample is cooled down to 40 K at $H=0$, then after waiting for thermal equilibrium, it is introduced in the magnet at 117.4 kOe to perform the NMR experiment. The ZFC procedure favors the AF CE state so that the FMM and the CE state coexist, whereas in the FC procedure, mainly the FMM phase exists. Indeed, the ZFC spectrum shows this coexistence since a line with $h_{loc} \sim 0$ corresponding to oxygen situated between AF correlated adjacent *ab* planes in the CE phase[19] is clearly seen. In the FC procedure, only the line corresponding to the FMM phase is detected. Furthermore the intensity of this line is larger compared to the ZFC spectrum. This demonstrates that the less intense line measured at 94 kOe cannot be due to regions with 3D AF structure (*A*-type or CE).

This line which intensity gradually increases below 130 K is rather consistent with poor FM order. Although the tendency of the field cooled $Nd_{0.5}Sr_{0.5}MnO_3$ to form the CO CE phase below 160 K still persists up to 120 kOe (see Fig. 11 of Ref. 3), it is not realized either on the macroscopic or on the microscopic scale, as demonstrated by ^{17}O NMR. Nevertheless, this tendency of Mn^{3+}-Mn^{4+} charge separation should create structural strains, which prevent locally the development of a well aligned FM order. As magnetic field increases, the tendency to form the CO CE order weakens allowing a better alignment of these Mn spins, as evidenced by the more symmetric shape of the line at 117.4 kOe.

IV. CONCLUSIONS

The magnetic order of the Mn spins was studied in the paramagnetic and ferromagnetic phases of $Nd_{0.5}Sr_{0.5}MnO_3$ by ^{17}O NMR at high magnetic field. The sample is an almost single phase material in accordance with the bulk magnetization data.

In the paramagnetic (PI) phase, the thermal behavior of the macroscopic magnetization is typical of a uniform 3D paramagnet undergoing a FM transition. Nevertheless, the temperature dependent extra broadening of the ^{17}O NMR line clearly indicates that magnetic inhomogeneities exist in the PI phase far above the transition. It consists of regions where 2D static spin correlations of neighboring Mn are formed in the *ab* plane. We cannot distinguish whether these 2D CO and/or OO configurations come from the one in the *ab* plane of the CO CE structure or from the ferromagnetically ordered layers of the AFM *A*-type phase. We suggest that these regions where the symmetry at oxygen sites is different from the average magnetic symmetry are in a direct relationship with the nanoscale structurally correlated regions observed above T_C by x-ray[12,13] and neutron scatterings.[15] These regions where the average magnetic symmetry is broken due to correlated Mn spin may play an important role in magnetoresistive properties of the manganite.

^{17}O NMR results at 94 kOe directly show that the FMM state of $Nd_{0.5}Sr_{0.5}MnO_3$ is rather inhomogeneous: regions with poor ferromagnetic order coexist with an almost perfect 3D FM spin order, so that at low T and high magnetic field where according to resistivity data[29] $Nd_{0.5}Sr_{0.5}MnO_3$ is in the FMM state the magnetic ordering is still far from being perfect. We suggest that this magnetic disorder originates from structural strains inside the FM domain. These strains exist both above and below the FMM-CO CE first order transition. This poor FM order is probably inherent to doped manganites even when the sample quality is very good.

ACKNOWLEDGMENTS

This work is supported by the Russian Foundation for Basic Research (Grants No. 05-02-16645, No. 06-02-17386, and No. 06-02-91171) and at Rutgers by the NSF Grant No. DMR-0405682. S.V. and A.Y. are grateful to ESPCI for hospitality and support.

[1] M. Salamon and M. Jaime, Rev. Mod. Phys. **73**, 583 (2001).
[2] E. Dagotto, New J. Phys. **7**, 67 (2005).
[3] Y. Tokura, Rep. Prog. Phys. **69**, 797 (2006).
[4] J. Goodenough, Phys. Rev. **100**, 564 (1955).
[5] E. O. Wollan and W. C. Koehler, Phys. Rev. **100**, 545 (1955).
[6] T. Fujiwara and M. Korotin, Phys. Rev. B **59**, 9903 (1999).
[7] R. Kajimoto, H. Yoshizawa, H. Kawano, H. Kuwahara, Y. Tokura, K. Ohoyama, and M. Ohashi, Phys. Rev. B **60**, 9506 (1999).
[8] R. Mahendiran, M. R. Ibarra, A. Maignan, F. Millange, A. Arulraj, R. Mahesh, B. Raveau, and C. N. R. Rao, Phys. Rev. Lett. **82**, 2191 (1999).
[9] P. Woodward, D. Cox, T. Vogt, C. Rao, and A. Cheetham, Chem. Mater. **11**, 3528 (1999).
[10] C. Ritter, R. Mahendiran, M. R. Ibarra, L. Morellon, A. Maignan, B. Raveau, and C. N. R. Rao, Phys. Rev. B **61**, R9229 (2000).
[11] J. Geck, D. Bruns, C. Hess, R. Klingeler, P. Reutler, M. v. Zimmermann, S.-W. Cheong, and B. Buchner, Phys. Rev. B **66**, 184407 (2002).
[12] V. Kiryukhin, B. G. Kim, T. Katsufuji, J. P. Hill, and S.-W. Cheong, Phys. Rev. B **63**, 144406 (2001).

[13] V. Kiryukhin, T. Y. Koo, A. Borissov, Y. J. Kim, C. S. Nelson, J. P. Hill, D. Gibbs, and S.-W. Cheong, Phys. Rev. B **65**, 094421 (2002).
[14] V. V. Krishnamurthy, I. Watanabe, K. Nagamine, H. Kuwahara, and Y. Tokura, Phys. Rev. B **61**, 4060 (2000).
[15] H. Kawano-Furukawa, R. Kajimoto, H. Yoshizawa, Y. Tomioka, H. Kuwahara, and Y. Tokura, Phys. Rev. B **67**, 174422 (2003).
[16] G. M. Zhao, K. Conder, H. Keller, and K. A. Muller, Nature (London) **381**, 676 (1996).
[17] G. M. Zhao, D. J. Kang, W. Prellier, M. Rajeswari, H. Keller, T. Venkatesan, and R. L. Greene, Phys. Rev. B **63**, 060402(R) (2000).
[18] A. Yakubovskii, K. Kumagai, Y. Furukawa, N. Babushkina, A. Taldenkov, A. Kaul', and O. Gorbenko, Phys. Rev. B **62**, 5337 (2000).
[19] A. Yakubovskii, A. Trokiner, S. Verkhovskii, A. Gerashenko, and D. Khomskii, Phys. Rev. B **67**, 064414 (2003).
[20] A. Trokiner, A. Yakubovskii, S. Verkhovskii, A. Gerashenko, and D. Khomskii, Phys. Rev. B **74**, 092403 (2006).
[21] S. Fraga, J. Karwowski, and K. Saxena, *Handbook of Atomic Data* (Elsevier Scientific, Amsterdam, 1976).
[22] E. Turov and M. Petrov, *Nuclear Magnetic Resonance in Ferro- and Antiferromagnets* (Halsded, New York, 1972), p. 207.
[23] R. Watson and A. Freeman, in *Hyperfine Interactions*, edited by A. J. Freeman and R. B. Frankel (Academic, New York, 1967), p. 345.
[24] A. Trokiner *et al.*, Phys. Rev. B **72**, 054442 (2005).
[25] G. Carter, L. Bennett, and D. Kahan, in *Progress in Material Science*, edited by B. Chalmers, J. W. Christian, and T. B. Massalski (Pergamon, Oxford, 1977), p. 33.
[26] B. Silbernagel, V. Jaccarino, P. Pincus, and J. Wernick, Phys. Rev. Lett. **20**, 1091 (1968).
[27] G. Allodi, R. DeRenzi, F. Licci, and M. W. Pieper, Phys. Rev. Lett. **81**, 4736 (1998).
[28] G. Allodi, R. DeRenzi, M. Solzi, K. Kamenev, G. Balakrishnan, and M. W. Pieper, Phys. Rev. B **61**, 5924 (2000).
[29] H. Kuwahara, Y. Tomioka, A. Asamitsu, Y. Moritomo, and Y. Tokura, Science **270**, 961 (1995).
[30] F. Keffer, in *Handbuch der Physik*, edited by S. Flügge and H. P. J. Wijn (Springer-Verlag, Berlin, 1966), Vol. 18/2.
[31] A. I. Akhiezer, V. G. Bar'yakhtar, and M. I. Kaganov, Sov. Phys. Usp. **3**, 567 (1960).
[32] H. Figiel, N. Spiridis, C. Kapusta, C. Wachter, and E. Dorman, Phys. Lett. A **211**, 377 (1996).
[33] I. Nakai and T. Fukagawa, J. Phys. Soc. Jpn. **62**, 2456 (1993).
[34] M. Jaime, P. Lin, M. B. Salamon, and P. D. Han, Phys. Rev. B **58**, R5901 (1998).
[35] The order of magnitude of the ^{17}O-^{16}O isotope effects on transition temperatures can be compared to ^{18}O-^{16}O isotope effects data in other manganites (Ref. 1). The comparison shows that these effects are indeed small in our case since isotope effects are proportional to the mass difference and, quantitatively, the ^{18}O isotope concentration is usually far larger than ^{17}O concentration in the present study.
[36] In the charge ordered state, the NMR line due to the oxygen sites situated between adjacent *ab* planes occurs at $h_{\mathrm{loc,apic}} \sim 0$. This NMR line is observable at nonzero magnetic field $H \geqslant 20$ kOe but impossible to detect at $H=0$.